Chapter 7: *Subseasonal Forecasting* - Lead Author Wassila M. Thiaw

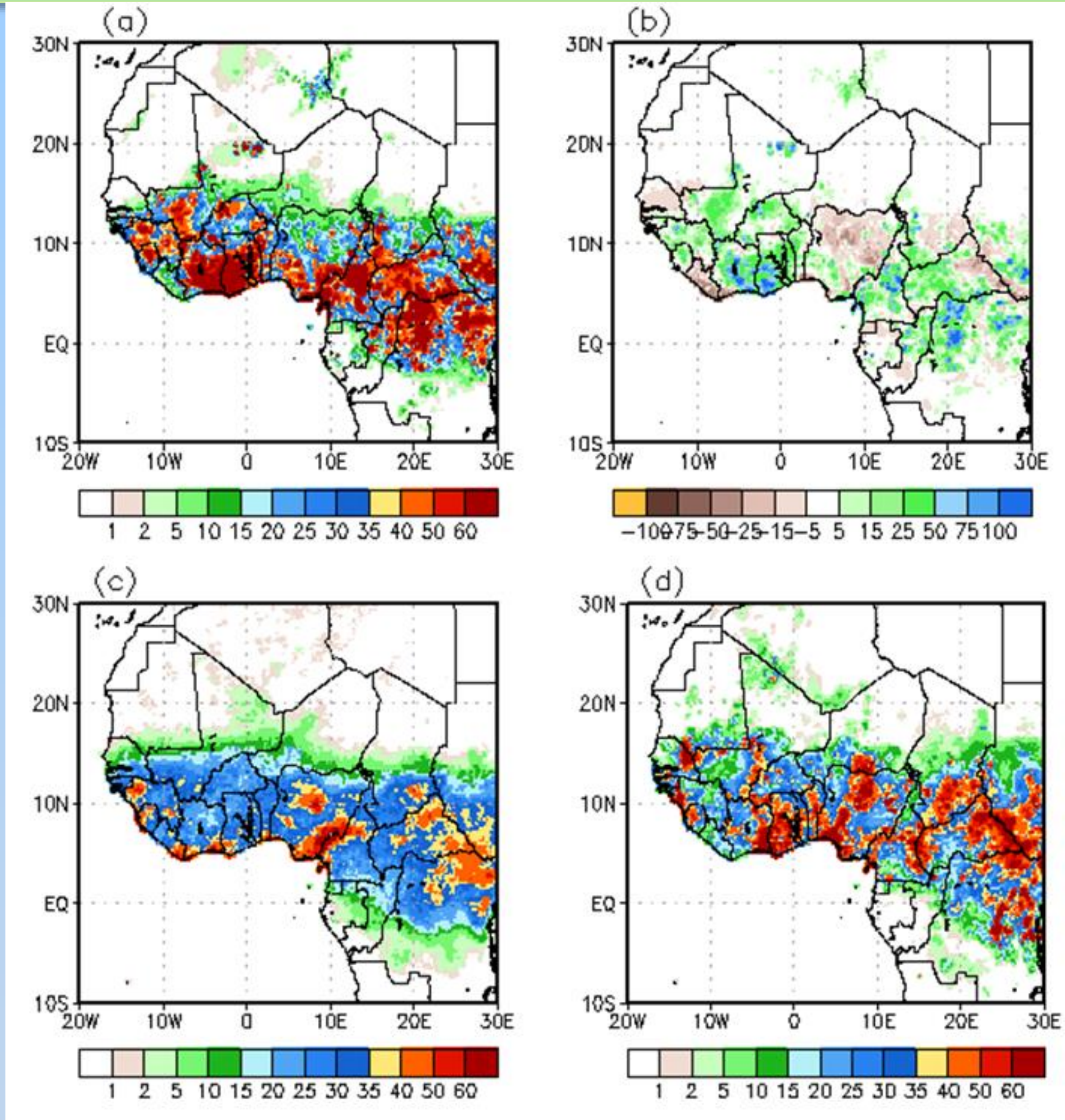

Figure 7.1: Satellite derived daily rainfall estimates (mm) from the blended gauge-satellite IR African Rainfall Climatology (ARC2; 1983 – 2012) dataset for
(a) rainfall total for 12 – 18 June 2012;
(b) rainfall anomaly for 12 – 18 June (1983 – 2012);
(c) rainfall climatology for the week of 19 – 25 June; and
(d) rainfall total for 19 – 25 June 2012.

Chapter 7: *Subseasonal Forecasting* - Lead Author Wassila M. Thiaw

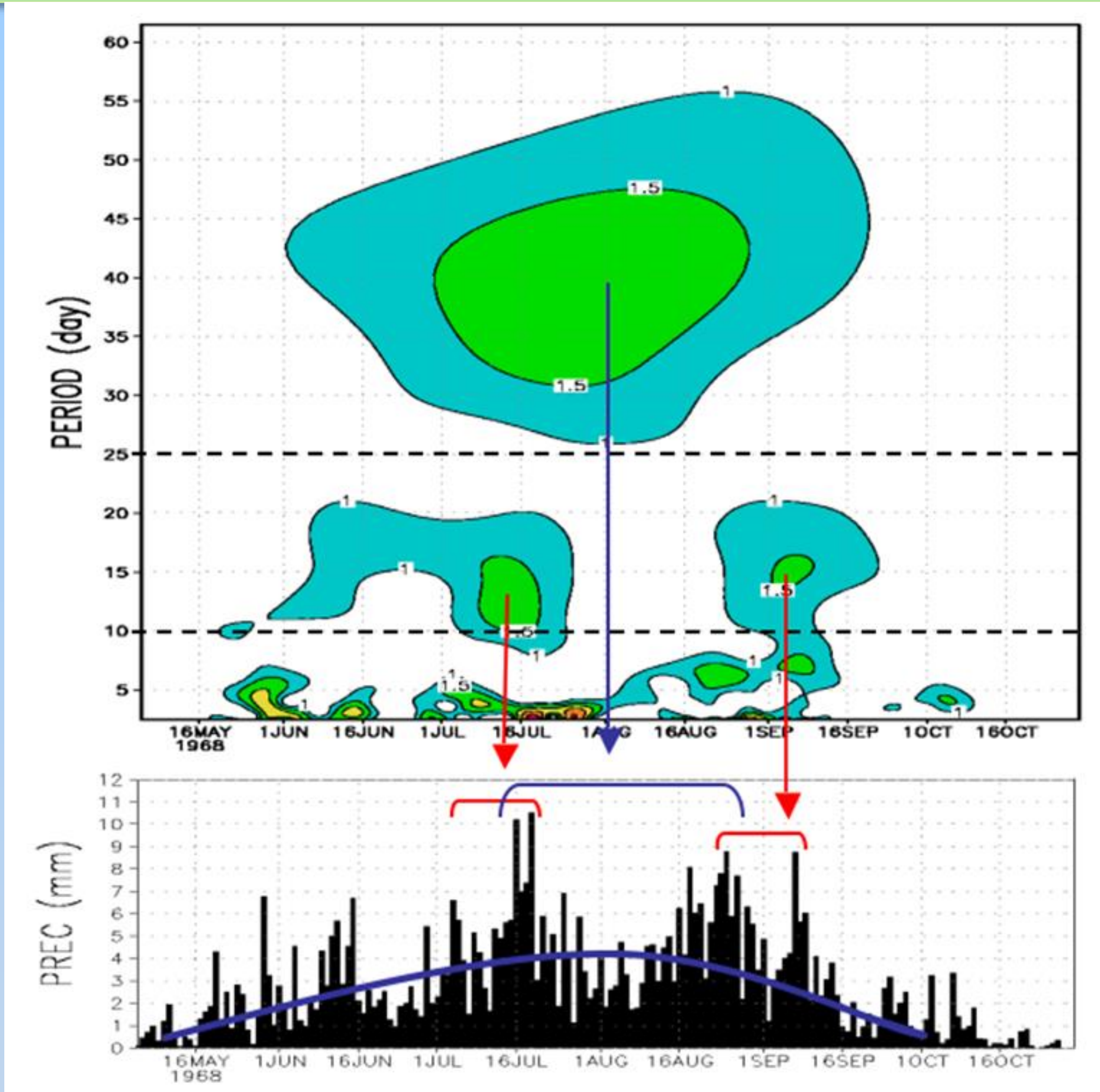

Figure 7.2:
Bottom: Daily rainfall time series (mm) from 1 May to 31 October 1968 averaged over 10°W-10°E/12.5°N-15°N. The smooth blue line represents the low-passed rainfall data.

Top: Wavelet analysis of the daily rainfall time series. Only periods lower than 60 days are presented. Values lower than 1 are not displayed. Sequences of 15-day and 40-day high variance are highlighted in red and blue respectively.

(Figure 1 from Janicot and Sultan, 2001.)

African Monsoon Multidisciplinary Analysis

ACMAD

WMO

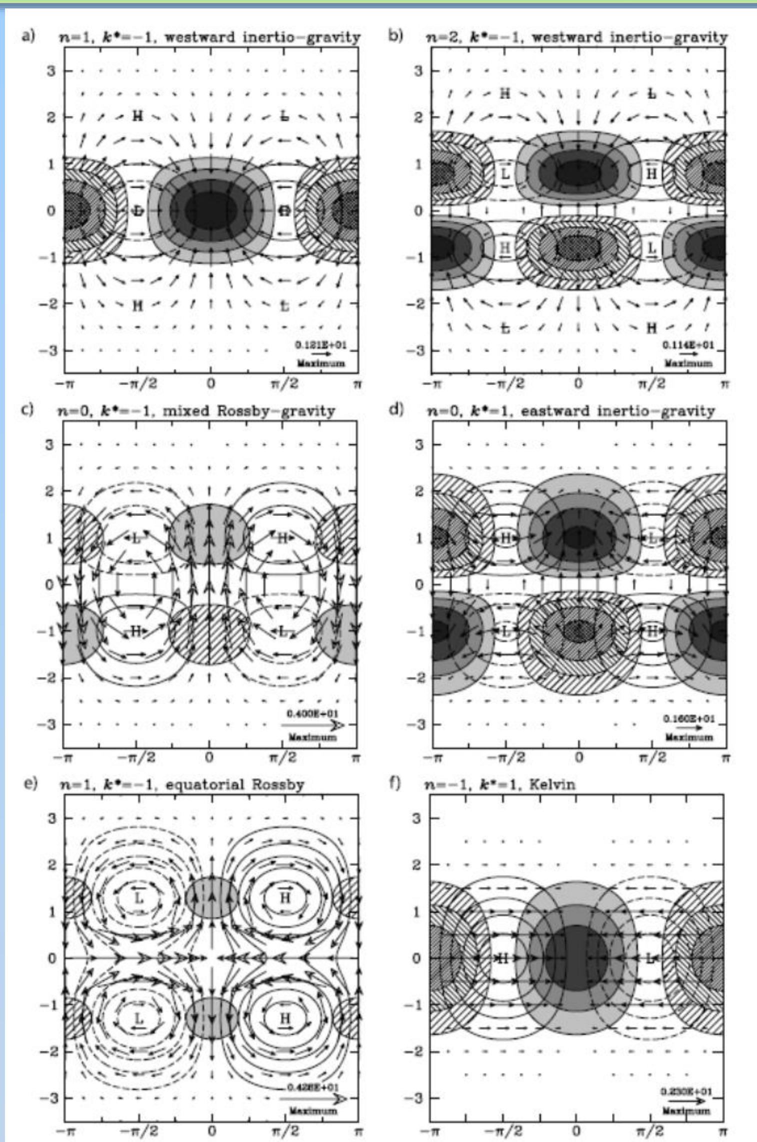

Figure 7.3: Horizontal structures of a subset of the zonally propagating wave solutions to the shallow water equations. Each is shown for a non-dimensional zonal wave number, $k^* = \pm 1$. All scales and fields have been non-dimensionalised.

The Equator runs through the centre of each diagram. Hatching is for divergence and shading is for convergence, with a 0.6 unit interval between successive levels. Unshaded contours are geopotential, with a contour interval of 0.5 units. Negative contours are dashed and the zero contour is omitted.

The maximum wind vectors in each panel are specified in the bottom right corner. (See Figure 3 from Kiladis et al., 2009 for more details.)

Chapter 7: *Subseasonal Forecasting* - Lead Author Wassila M. Thiaw

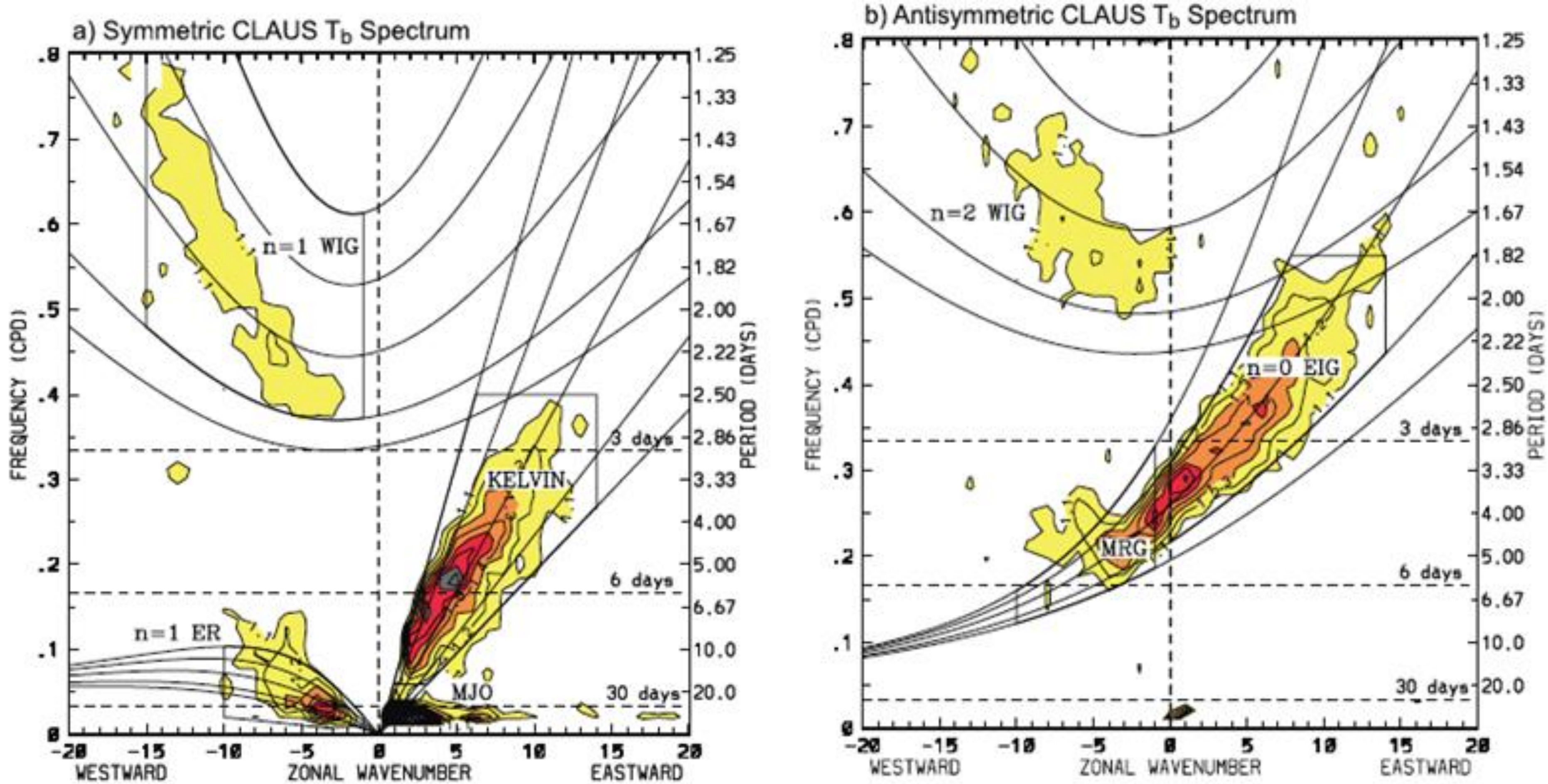

Figure 7.4: Wave number-frequency power spectrum for symmetric (left) and antisymmetric (right) spectrum of brightness temperature (Tb) from the European Cloud Archive User Services for July 1983-2005, averaged over 15N, 15S. (Figure 1 from Kiladis et al., 2009.

Chapter 7: *Subseasonal Forecasting* - Lead Author Wassila M. Thiaw

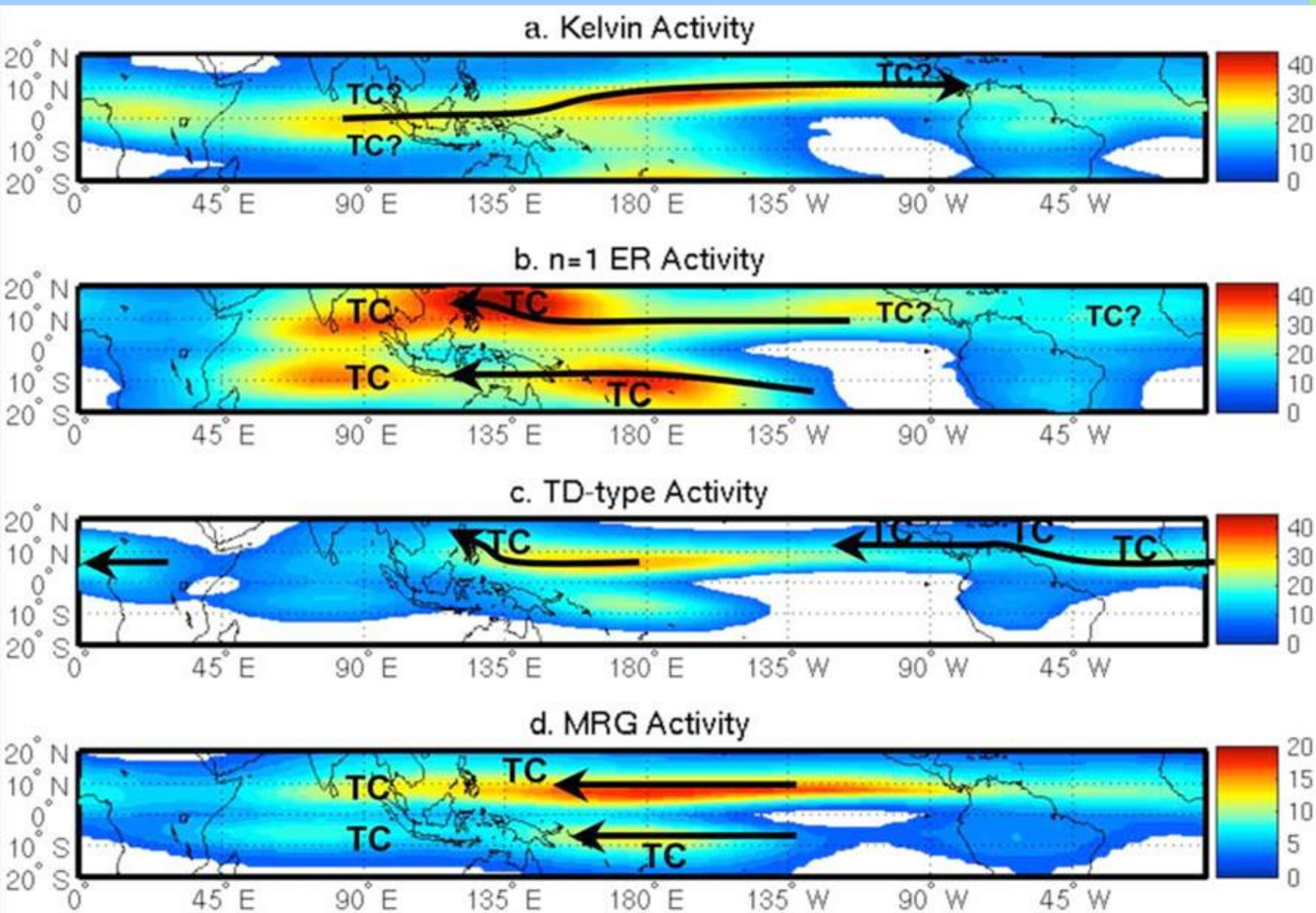

Figure 7.5: Distribution of annual mean variance of CLAUS brightness temperature (TB) filtered for the (a) Kelvin, (b) n = 1 ER, (c) tropical depression (TD), and (d) MRG wave bands.

Also shown are preferred direction of propagation and preferred location of tropical cyclone (TC) genesis associated with each mode.

(From Figure 5 from Kiladis et al., 2009.)

African Monsoon Multidisciplinary Analysis

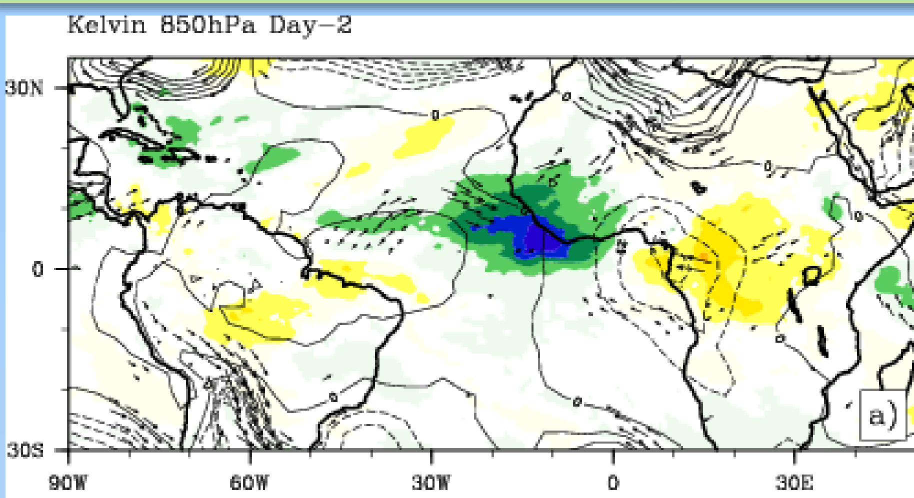

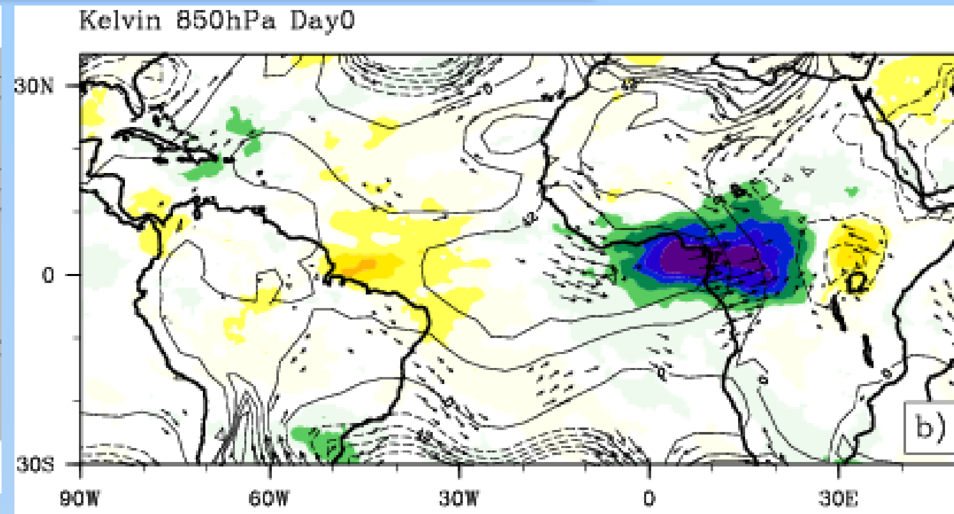

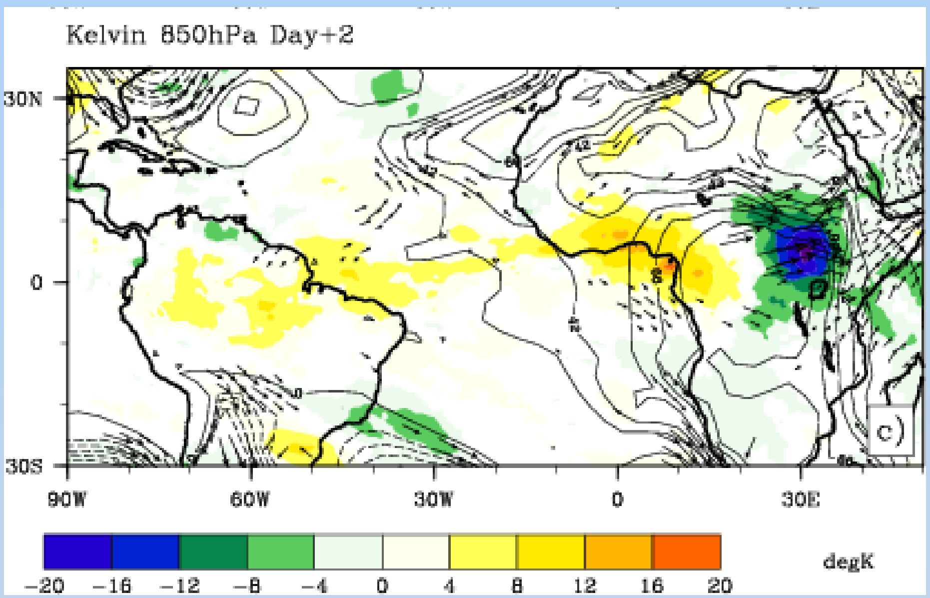

Figure 7.6: Composite maps of May to October anomalous brightness temperature (Tb) (shading), geopotential height (contours), and wind (vectors) associated with a -10 K perturbation in Kelvin wave Tb at the base point 2°N, 10°E, for (a) day –2 at 850 hPa, (b) day 0 at 850 hPa, and (c) day +2 at 850 hPa.

Chapter 7: *Subseasonal Forecasting* - Lead Author Wassila M. Thiaw

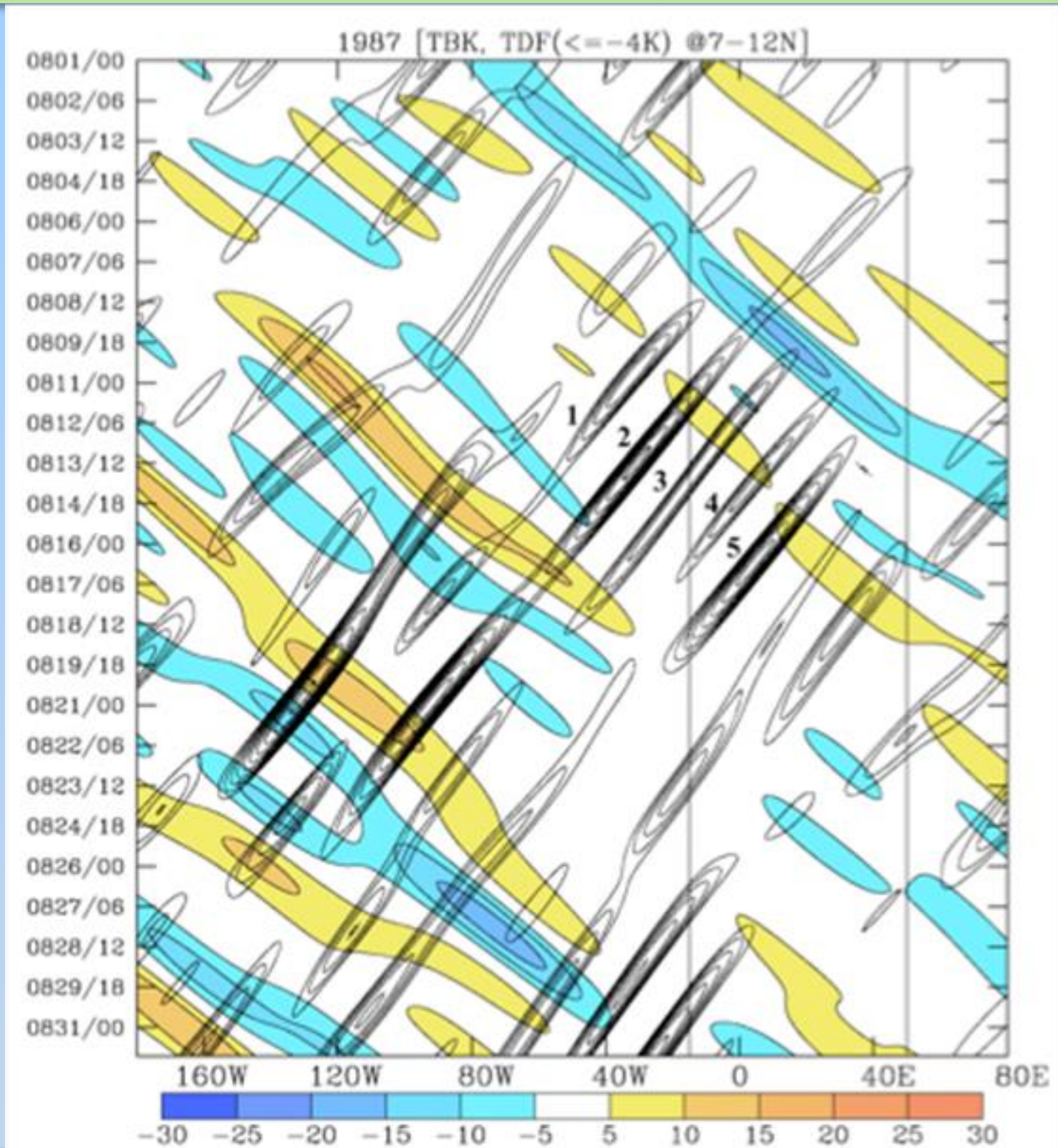

Figure 7.7: Kelvin-filtered cloud brightness temperature (TB; shaded) and AEWs (contoured every 2 K from -4 K; only negatives shown for clarity) for August 1987, averaged between the 7◦ - 12◦N range.

AEWs are determined by filtering TB in the period of 2–7.5 days and westward wavenumber 6–20. Numbers 1–5 denote the AEWs initiated or enhanced in association with the enhanced phase of the Kelvin wave.

(From Mekonnen et al., 2008)

African Monsoon Multidisciplinary Analysis

Chapter 7: *Subseasonal Forecasting* - Lead Author Wassila M. Thiaw

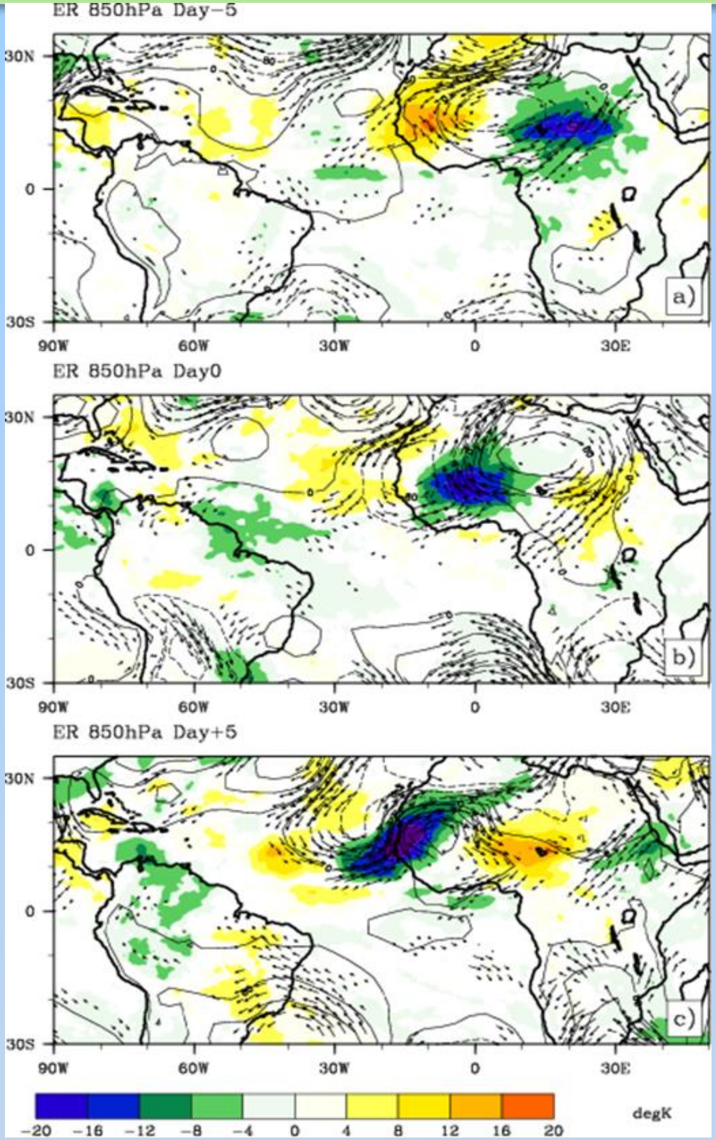

Figure 7.8: Composite maps of May to October anomalous brightness temperature (Tb) (shading), geopotential height (contours), and wind (vectors) associated with a -7.5 K perturbation in n = 1 ER wave Tb at the base point 15◦N, 0◦E, for (a) day −5 at 850 hPa, (b) day 0 at 850 hPa, and (c) day +5 at 850 hPa.

The contour interval is 40 mgp, with negative contours dashed. Cold shading is for negative and warm shading if for positive Tb perturbations. Tb and wind vectors are locally significant at the 95% level, with the largest vectors around 2 m s-1.

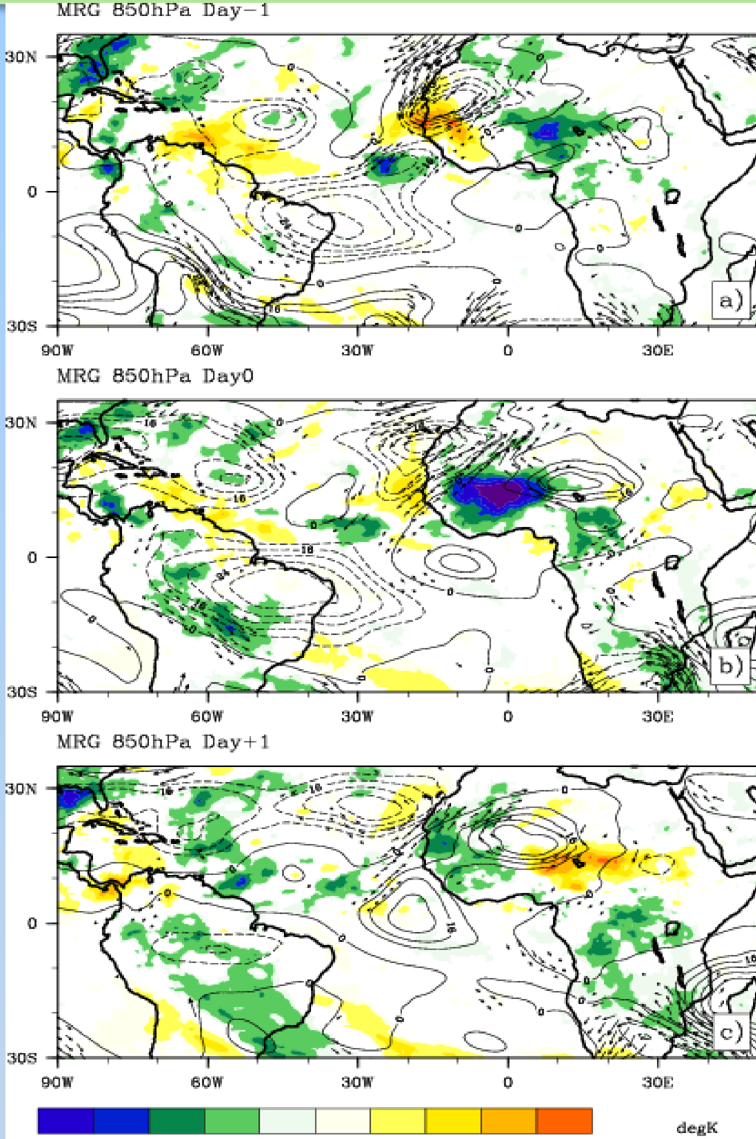

Figure 7.9: Composite maps of May to October anomalous (Tb) (shading), stream function (contours), and wind (vectors) associated with a -7.5 K perturbation in MRG wave Tb at the base point 15°N, 0°E, for (a) day -1 at 850 hPa, (b) day 0 at 850 hPa, and (c) day +1 at 850 hPa.

The contour interval is 4×105 m2 s-1, with negative contours dashed. Cold shading is for negative and warm shading is for positive Tb perturbations. Tb and wind vectors are locally significant at the 95% level, with the largest vectors around 2 m s-1.

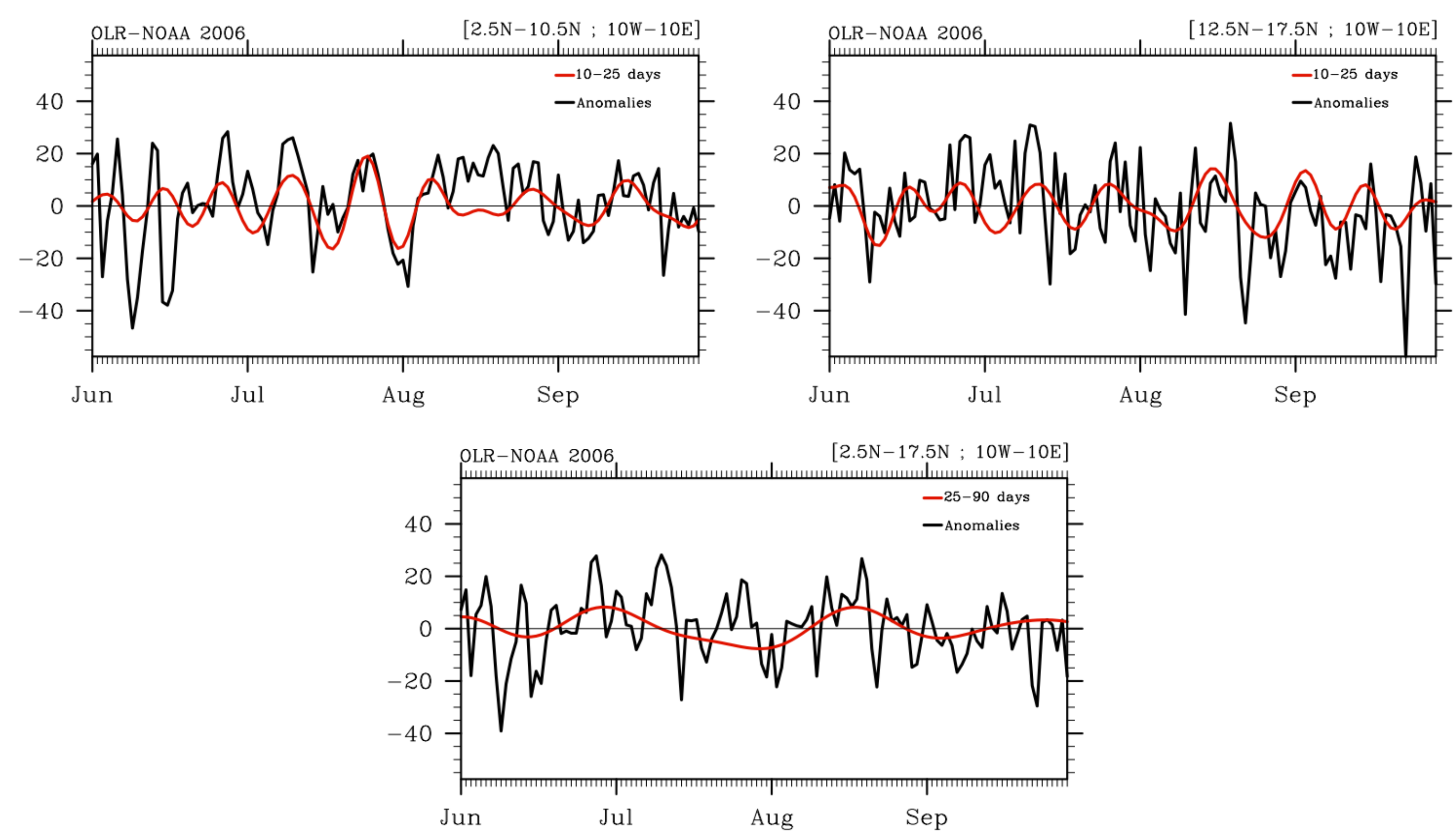

Figure 7.10: Time series of deseasonalised (black) and filtered (red) OLR indices (W.m-2) over 10°W–10°E in summer 2006:
Top right : Index averaged over 12.5°N–17.5°N and 10–25-day filtered values
Top left : Index averaged over 2.5°N–10°N and 10–25-day filtered values
Bottom : Index averaged over 2.5°N–17.5°N and 25–90-day filtered values

Chapter 7: *Subseasonal Forecasting* - Lead Author Wassila M. Thiaw

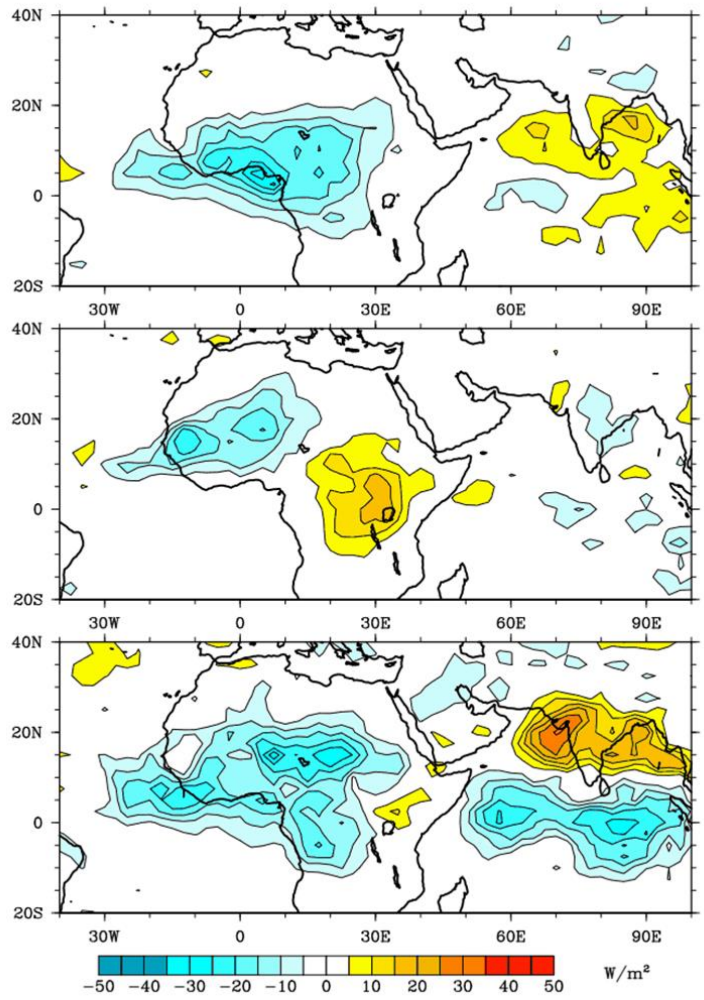

Figure 7.11: Composite pattern of the subseasonal modes in terms of non-filtered OLR modulation (W m-2): (top) quasi-biweekly zonal dipole (QBZD) mode; (middle) "Sahel mode" and (bottom) "MJO mode". Adapted from Sultan et al., 2003.

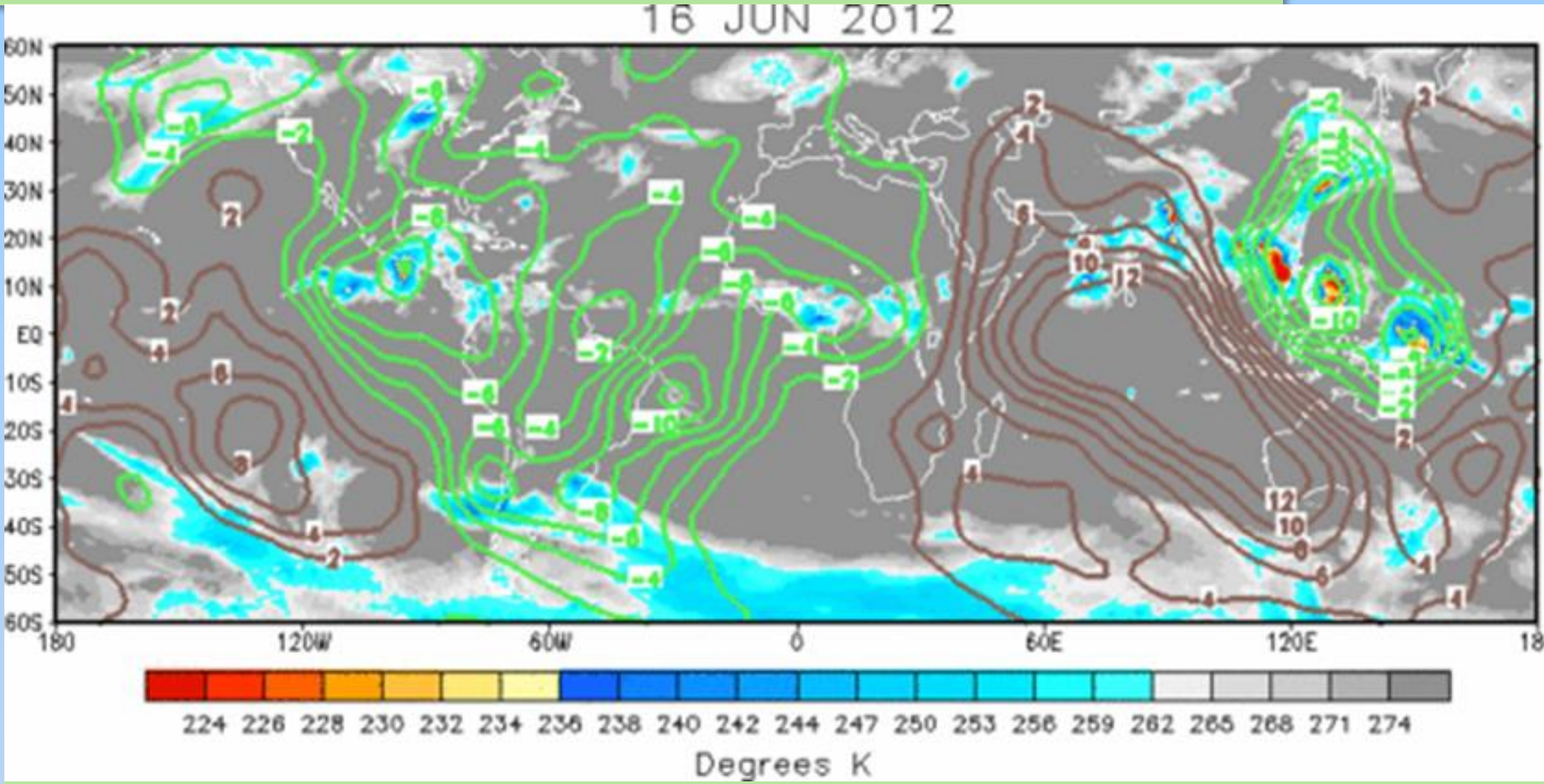

Figure 7.12: Outgoing longwave radiation (NOAA 18 AVHRR IR window channel measurements by NESDIS/ORA) for 16 June 2012, shading in K, overlaid with 200 hPa velocity potential contours. Contour interval is 106m2s. Low values of OLR are indicative of convection. Green (brown) contours are associated with upper level divergence (convergence). Source: NOAA's Climate Prediction Center MJO web portal: http://www.cpc.ncep.noaa.gov/products/precip/CWlink/MJO/mjo.shtml.

African Monsoon Multidisciplinary Analysis

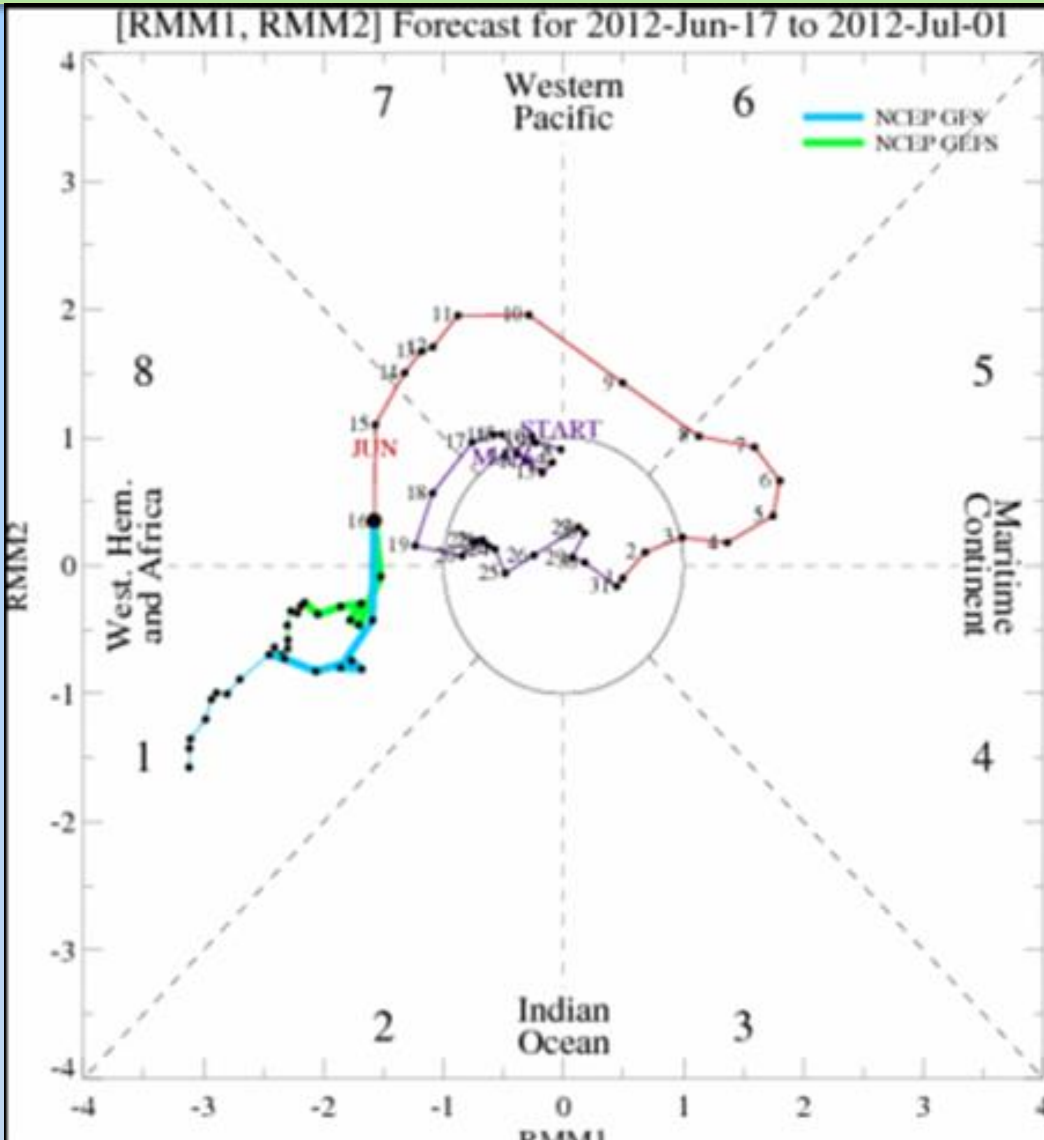

Figure 7.13: Phase-space representation of the two-component MJO index, for the period 1 May – 16 June 2012 (thin lines) and the forecast period valid 17 June – 1 July 2012. Each dot represents the value of the index on a particular day, with the starting and ending days labelled.
Also shown are the eight defined phases of the MJO and the region used to signify weak MJO activity. Also labelled (with words) are the approximate locations of the near-equatorial enhanced convective signal of the MJO for each quadrant of the phase space (e.g., the "Indian Ocean" for phases 2 and 3).

After Wheeler and Hendon (2004).
Source: NOAA's Climate Prediction Center MJO web portal: http://www.cpc.ncep.noaa.gov/products/precip/CWlink/MJO/mjo.shtml.

African Monsoon Multidisciplinary Analysis

ACMAD

WMO

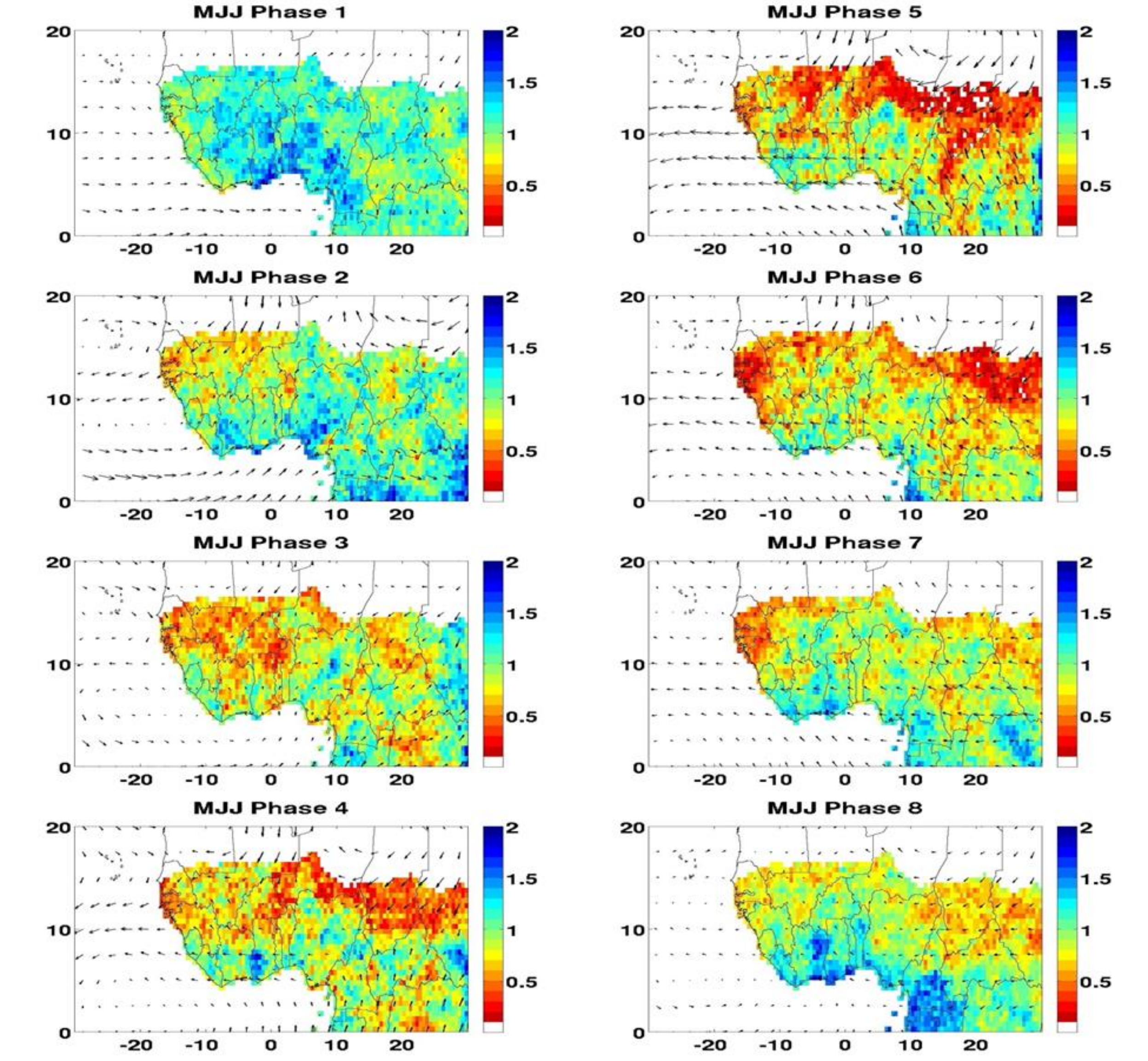

Figure 7.14: MJO composites of weekly rainfall probabilities (contours and shading) and 850-hPa wind anomalies (vectors) for the MJJ season for phases 1–8.

Rainfall probabilities refer to the chance of weekly rainfall exceeding the upper decile, expressed as a ratio with the mean probability (nominally 33%).

Adapted after Wheeler et al., 2009.

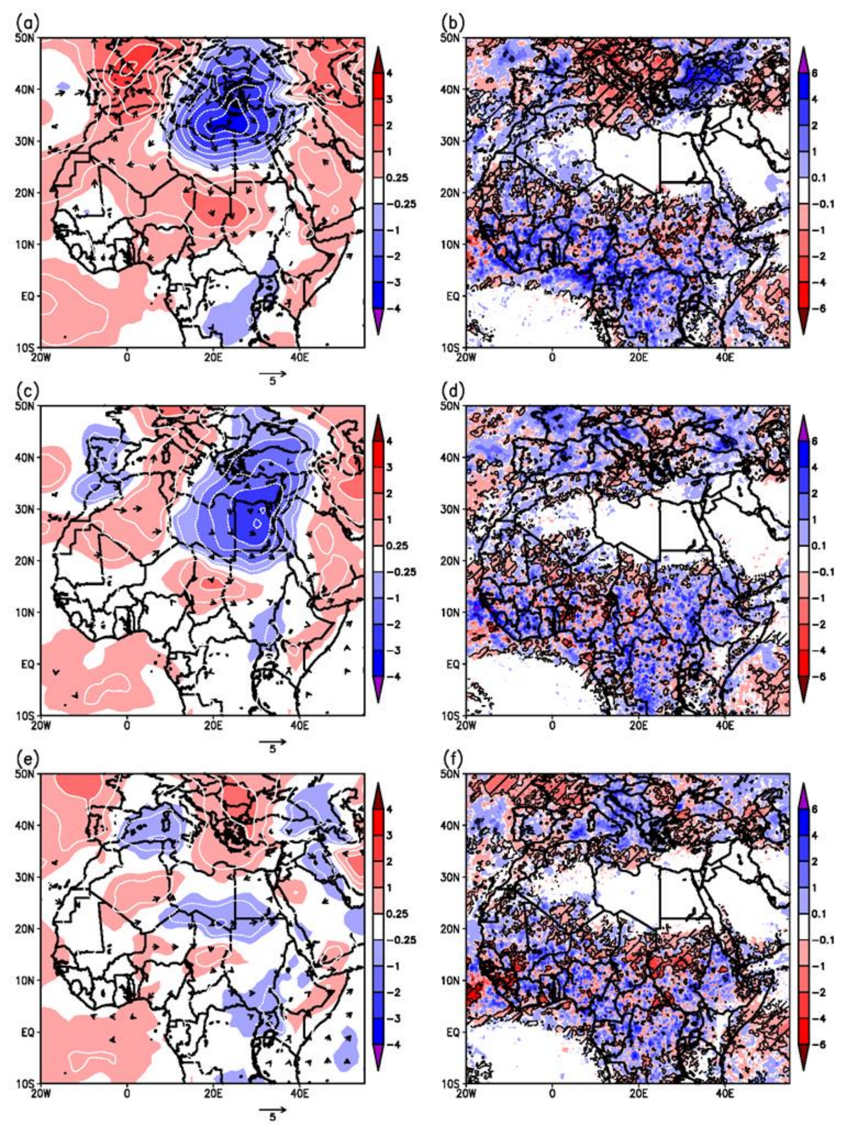

Figure 7.15: Summer-time (July – September) daily composites of cold air surges.
(Left column) 850 hPa temperature (K) and wind (m s-1) anomalies, and (right column) NASA TRMM 3B42V7 precipitation anomalies (mm day-1) at composite Day 0 (a & b), Day+2 (c & d), and Day+5 (e & f). Day 0 is defined as the date when the equatorward moving 850 hPa cold temperature anomaly averaged between 10°E - 30°E associated with a cold air surge has first crossed 30°N.
Hatching denotes rainfall anomalies statistically significant at the 90% level of confidence. Only statistically significant wind vectors at the 95% level of confidence are shown.

Adapted from Vizy and Cook, 2014.

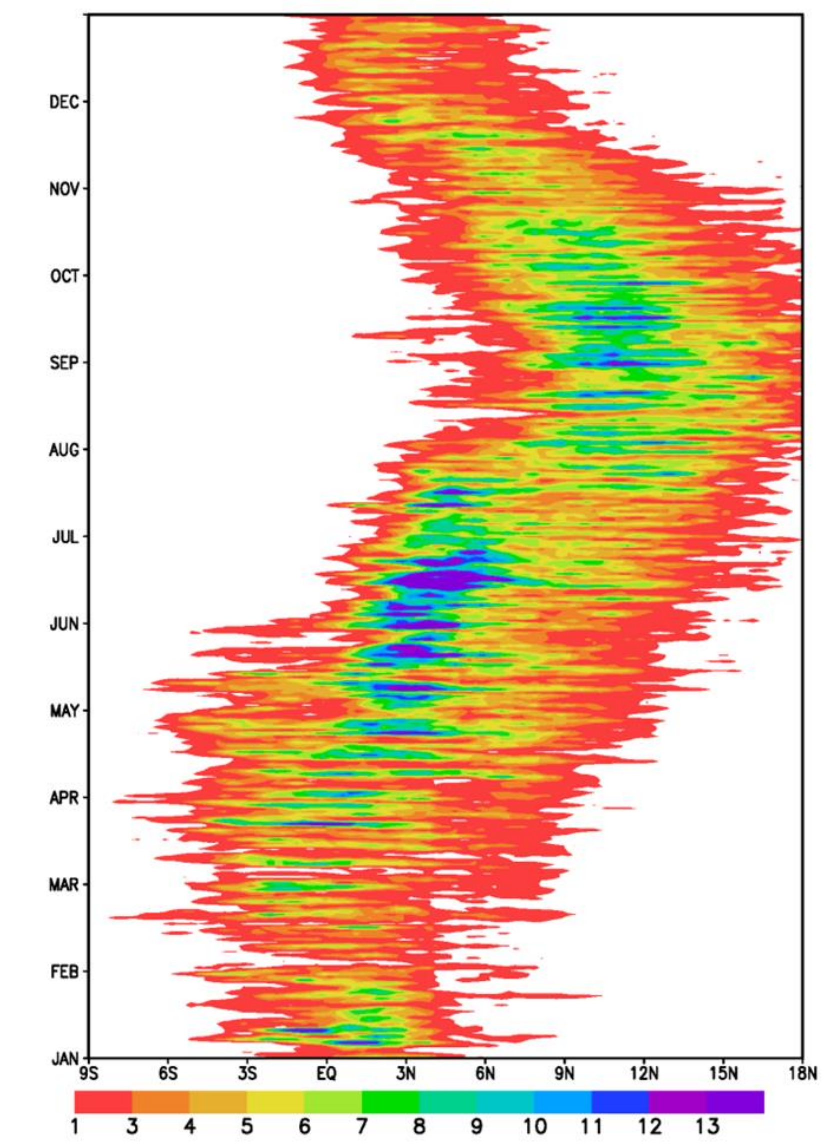

Figure 7.16: Daily precipitation climatology (mm/day) for 1998-2012 from TRMM 3B42 V7 (Huffman et al., 2007).
This may be compared with Figure 1.3(b).

Chapter 7: *Subseasonal Forecasting* - Lead Author Wassila M. Thiaw

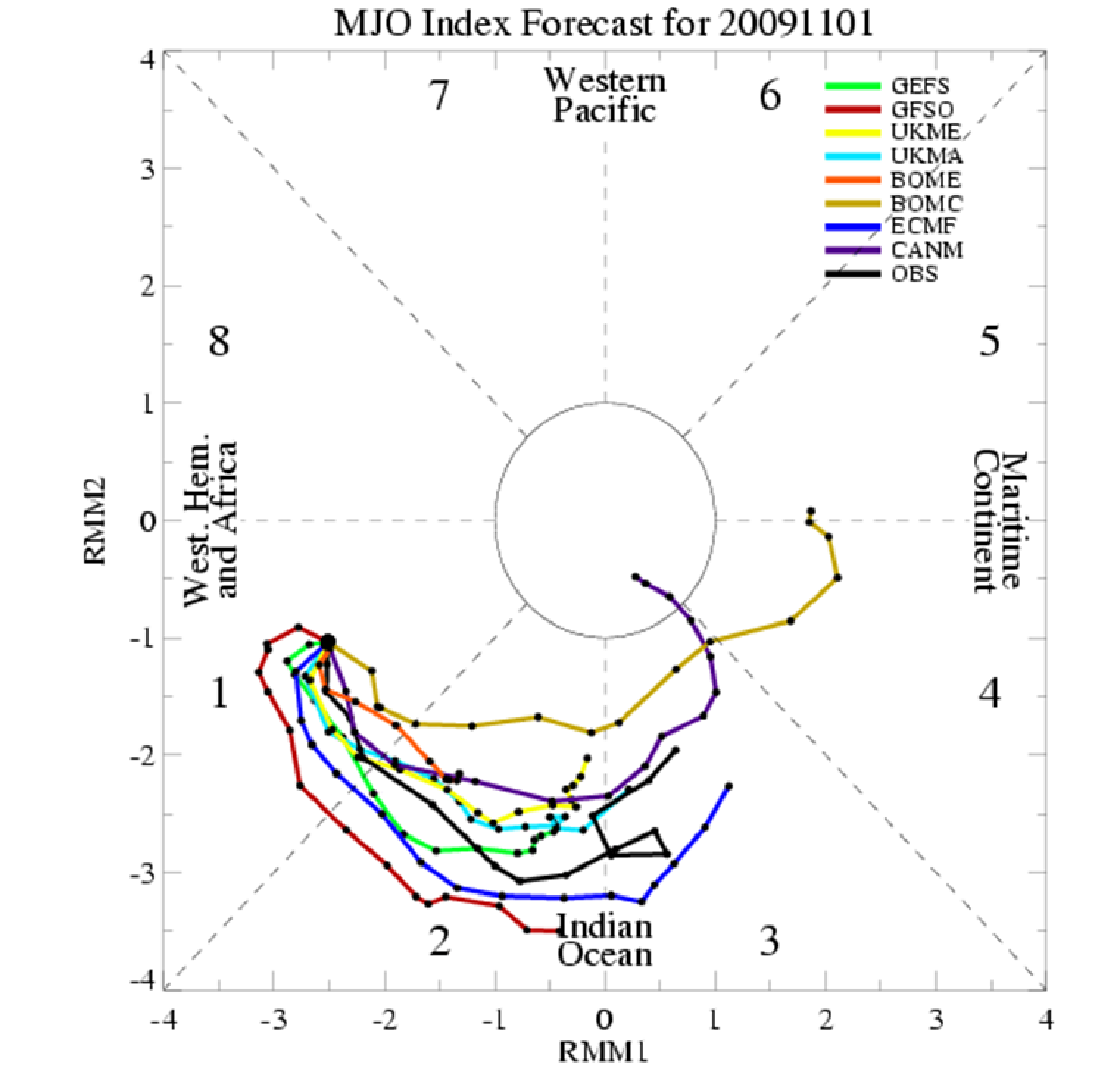

Figure 7.18: Two-component MJO index (as in Figure 7.13), for projections of the MJO Index from dynamical coupled ocean-atmosphere models, 1 November 2009 initial conditions, through week-2 forecasts.

Source: NOAA's Climate Prediction Center MJO web portal: http://www.cpc.ncep.noaa.gov/products/precip/CWlink/MJO/mjo.shtml

African Monsoon Multidisciplinary Analysis

Chapter 7: *Subseasonal Forecasting* - Lead Author Wassila M. Thiaw

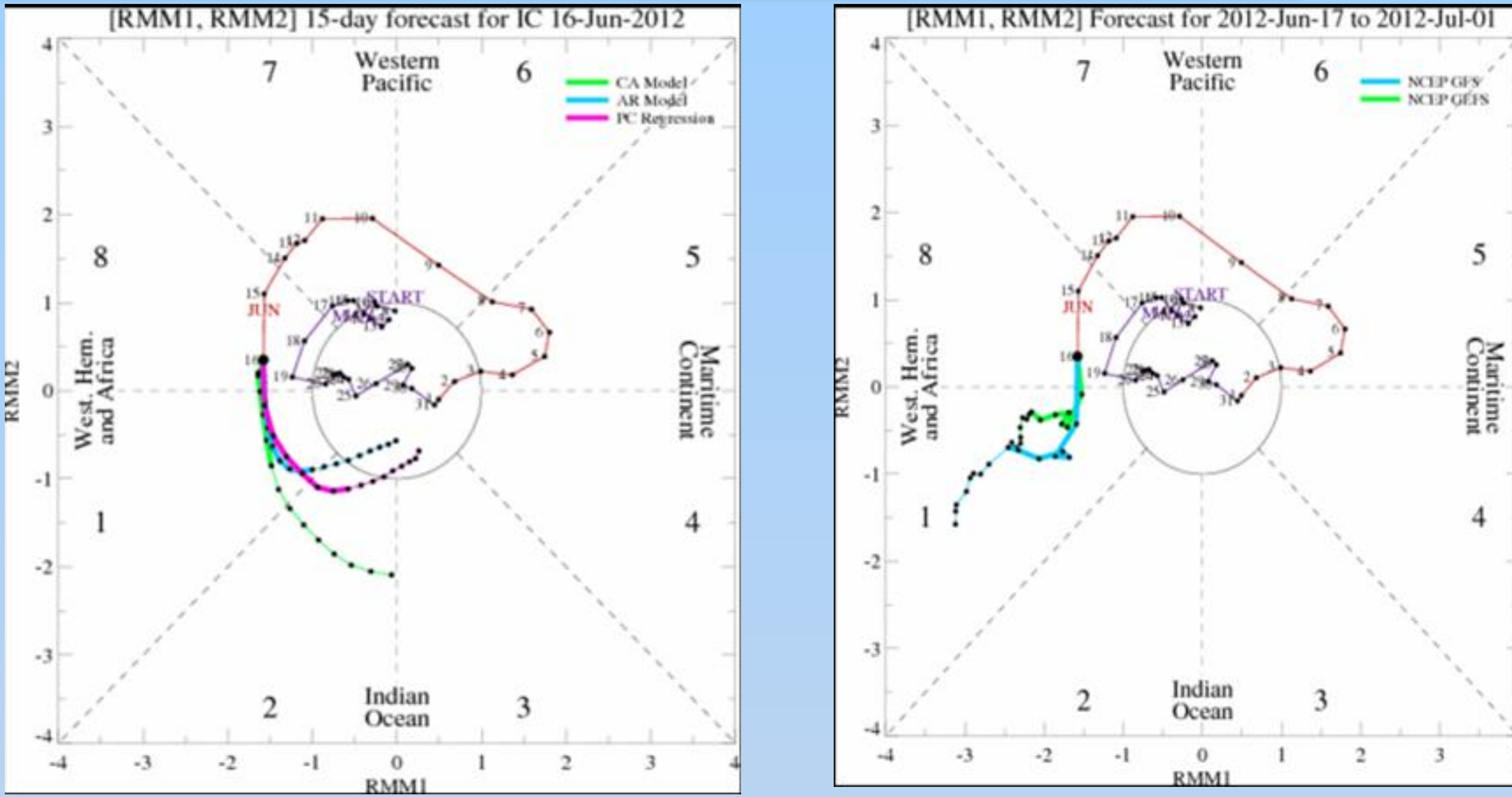

Figure 7.19: Plot of forecast two-component MJO index. The right panel is the same forecast as shown in Figure 7.13. The left panel includes statistical forecasts of the MJO index: Constructed analogs (green); autoregression model (blue); and principal component regression (pink). Source: NOAA’s Climate Prediction Center MJO web portal: http://www.cpc.ncep.noaa.gov/products/precip/CWlink/MJO/mjo.shtml

African Monsoon Multidisciplinary Analysis

ACMAD

WMO

Chapter 7: *Subseasonal Forecasting* - Lead Author Wassila M. Thiaw

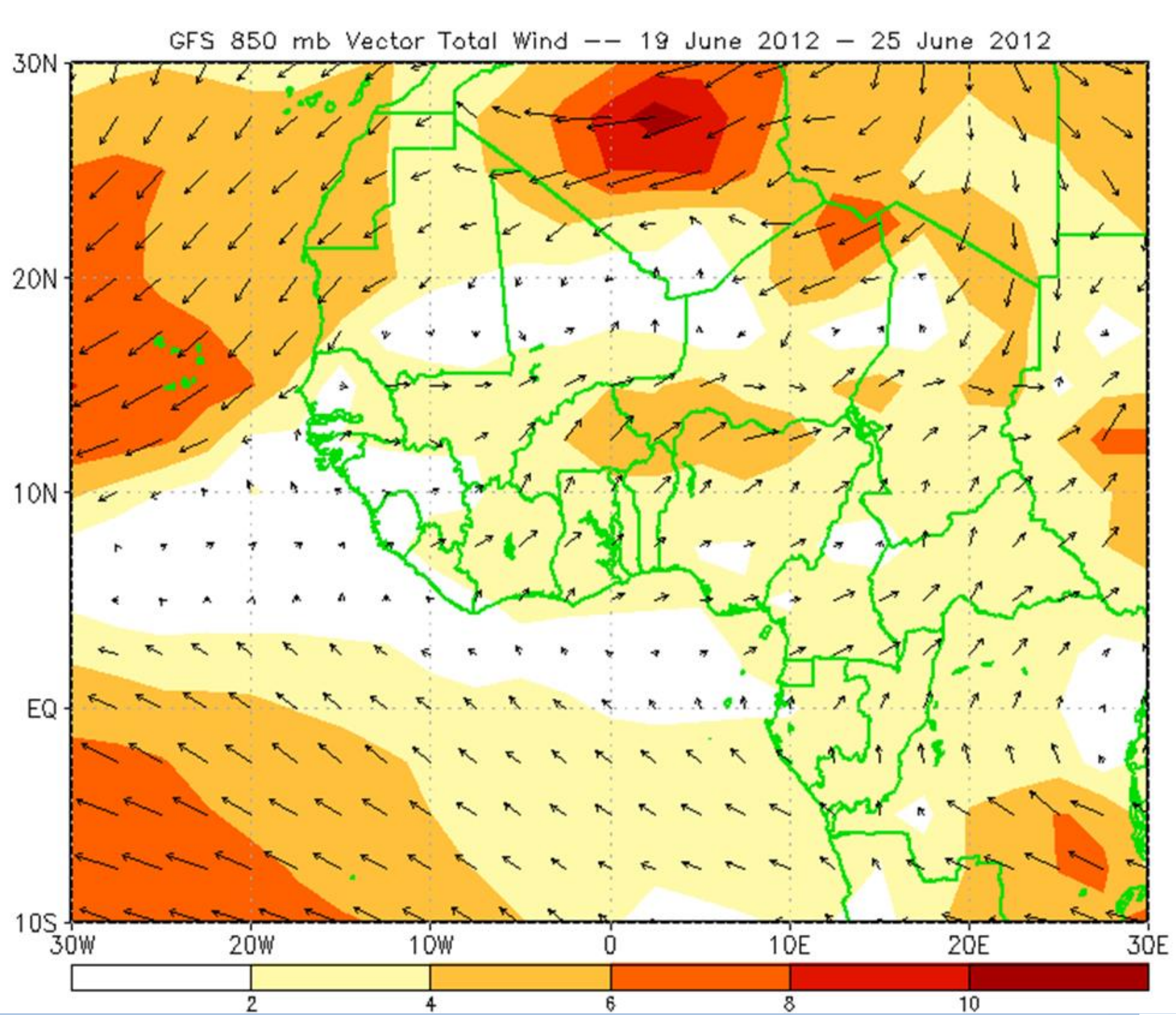

Figure 7.20: GFS 850hpa wind forecast (ms-1), valid June 19-25, 2012. Arrows indicate wind direction, and the magnitude of the wind is represented by the colour shades.

African Monsoon Multidisciplinary Analysis

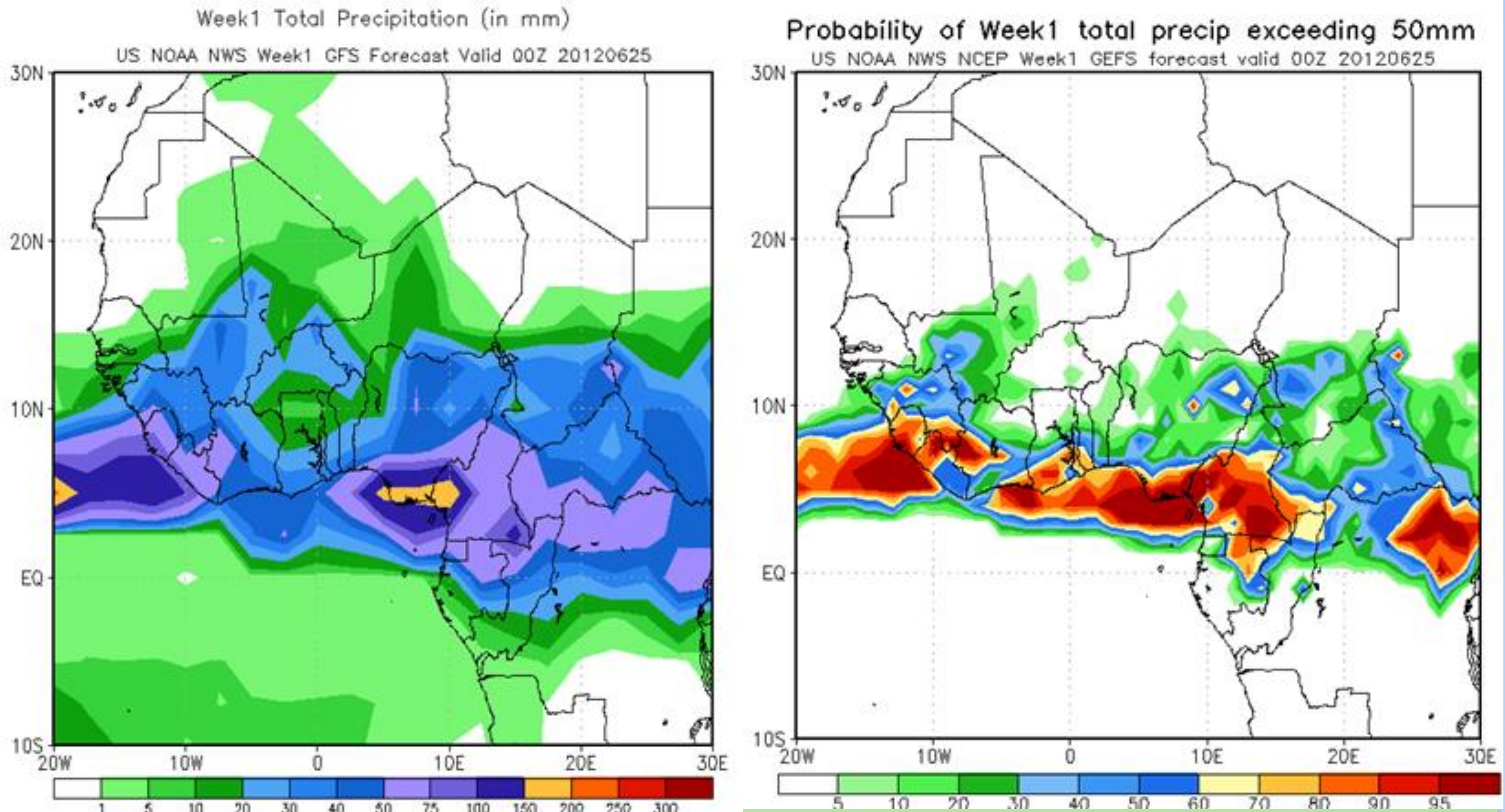

Figure 7.21: GFS 7-day Precipitation forecast, total in mm (left) and probability 7-day total precipitation exceeding 50 mm (right).

Chapter 7: *Subseasonal Forecasting* - Lead Author Wassila M. Thiaw

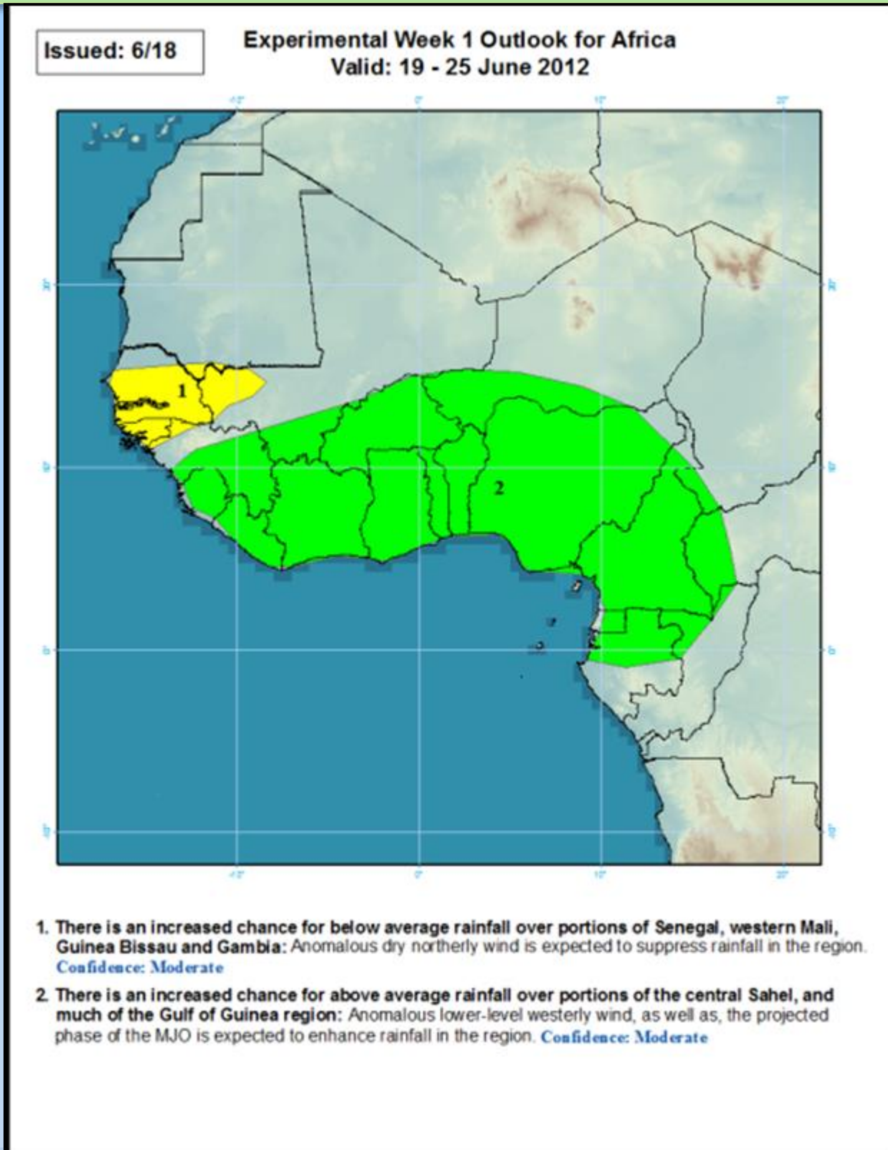

Figure 7.22: Week-1 precipitation outlook, valid 19-25 June 2012.

Green (yellow) shades indicate areas with a higher chance for above (below) average rainfall.

African Monsoon Multidisciplinary Analysis

Chapter 7: *Subseasonal Forecasting* - Lead Author Wassila M. Thiaw

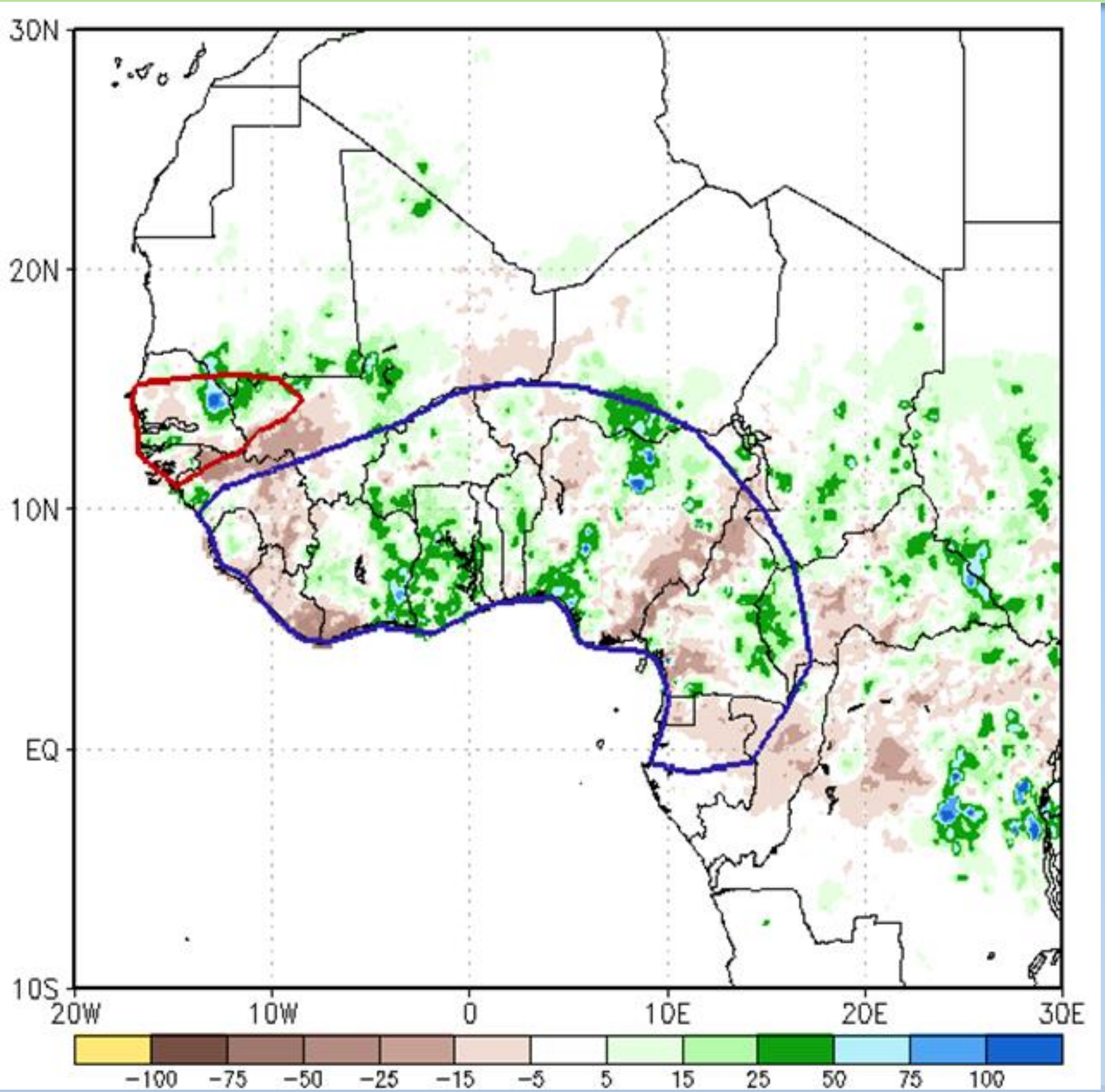

Figure 7.23: Satellite rainfall estimate (ARC2) anomaly (mm) for 19-25 June 2012 used in the verification of the week-1 outlook valid June 19 – 25, 2012.

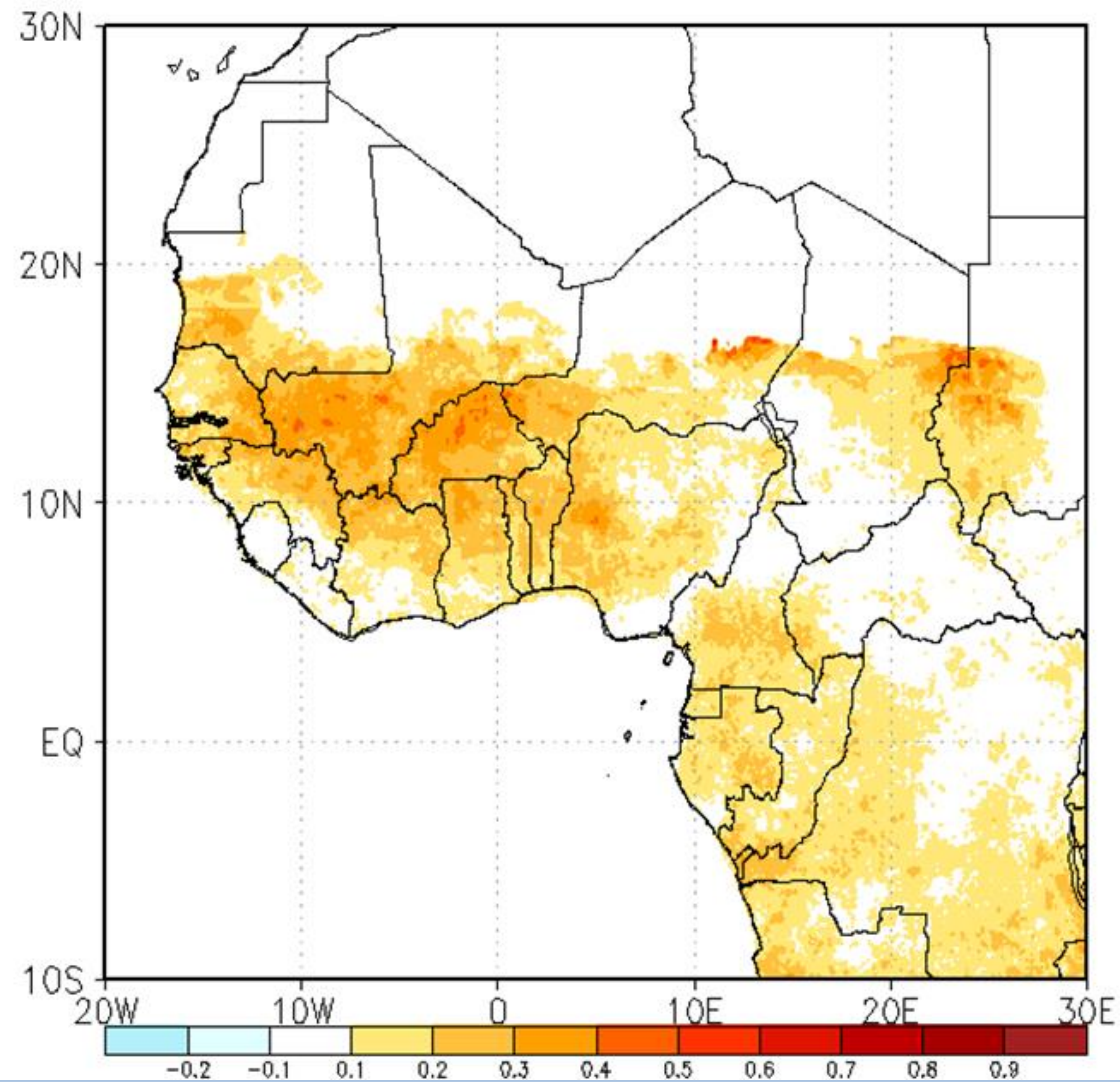

Figure 7.24: Heidke skill score for week-1 rainfall outlooks issued 14 April, 2008 through December 31, 2012.

Adapted from Thiaw and Kumar, 2015.